Deep Learning-Based Prediction Algorithm on Atmospheric Turbulence-Induced Wavefront for Adaptive Optics

Ning Wang, Licheng Zhu, Shuai Ma, Wang Zhao, Xinlan Ge, Zeyu Gao, Kangjian Yang, Shuai Wang, and Ping Yang

***Abstract*—Correction performance of an adaptive optics (AO) system is severely limited by its system latency under high temporal frequency distortions. Wavefront prediction methods has been proven to be an effective way to compensate system delay. A novel wavefront prediction method based on residual learning fusion network (RLFNet) is proposed in this paper. The network is able to eliminate redundant information between adjacent wavefront frames and fuse refined features, which provides a higher prediction accuracy under fewer priori wavefront input. The method is tested on a 1km laser atmospheric transmission experimental setup through high frequency atmospheric turbulence, where wavefront data is collected from a 1kHz Shack-Hartmann wavefront sensor (SHWS). We show that the proposed architecture is able to predict the second frame wavefront after the previous 6 frames with a root-mean-square (RMS) wavefront error reduction up to 53% compare to non-predictive method.**

***Index Terms*—Adaptive optics, atmospheric turbulence, neural network, wavefront prediction.**

I. Introduction

SUPPRESSING the degrading effect of atmospheric turbulence on laser beam transmission has been a major research focus in the fields of laser communications, and laser detection among others. AO technique is an effective way to compensate atmospheric turbulence in real time. However, real AO systems usually assume that the distorted wavefront is static during a control period, which leads to a servo-lag error of 2-3 sampling periods in the control loop [1], [2], [3]. The time delay in the loop mainly comes from signal processing and control tasks such as wavefront sensor data acquisition, wavefront reconstruction and control operation. Such time delay will cause the compensation wavefront on the deformable mirror (DM) lag behind the actual measured wavefront, which severely limits the correction performance of the AO system.

A large number of prediction methods have been studied to compensate the time delay. Among these prediction methods, the iterative prediction method like Recursive Least Squares (RLS) algorithm is to minimize the systematic error, which provides a simple calculation process and avoids to fall into the local minimum point. However, when the mode order of wavefront aberrations is too high, it cannot converge in a short time [4], [5]. Model-based prediction methods use atmospheric turbulence model to predict the change of wavefront, such as the Linear Quadratic Gaussian control algorithm, which has a good approximation performance, but it is difficult to balance the prediction accuracy of the model between the control complexity of the controller [6], [7], [8]. In addition, there are more complex Kalman Filter based methods [9], [10], [11], [12] and extensions of various approach [13], [14], [15], [16]. In fact, the majority of these algorithms can be described as analytical applications of various estimation frameworks. But amid a large wave of general advances in Neural-network (NN), NN-based methods have been widely used for wavefront reconstruction and prediction of AO systems [17], [18]. It turns out that NN-based methods have the advantage over analytical estimation techniques in terms of alleviating time delay, because NN predictors are self-optimizing, generalizable and have strong nonlinear fitting ability [18], [19]. Shi Xiaoyu [20] and Yan Zaojun [21] et al. used a two-layer back-propagation (BP) neural network prediction algorithm to predict the open-loop control voltage of the DM, and the correction effect was about 30 times better than that of the RLS algorithm for the same wind speed. In 2020, Chen Ying et al. used Long Short-term Memory (LSTM) network for voltage prediction, and its prediction residual was about 8 times lower than that of BP network [22].

In terms of network input and output types, direct prediction of the wavefront can be more advantageous, because the prediction model is largely unaffected by changes in SHWS and DM, thus, there is no need to design specific network models for different AO systems. Therefore, the way of directly predicting

Manuscript received 12 July 2022; revised 21 August 2022; accepted 31 August 2022. Date of publication 5 September 2022; date of current version 29 September 2022. This work was supported in part by the National Natural Science Foundation of China under Grant 62105336, and in part by the Sichuan Province Science and Technology Support Program of China under Grant 2022JDRC0095. *(Corresponding authors: Licheng Zhu; Ping Yang.)*

Ning Wang, Shuai Ma, and Xinlan Ge are with the Key Laboratory on Adaptive Optics, Chinese Academy of Sciences, Chengdu 610209, China, with the Institute of Optics and Electronics, Chinese Academy of Sciences, Chengdu 610209, China, and also with the School of Electronic, Electrical and Communication Engineering, University of Chinese Academy of Sciences, Beijing 100049, China (e-mail: w_ning@163.com; msromam@163.com; 18189195675@163.com).

Licheng Zhu, Wang Zhao, Zeyu Gao, Kangjian Yang, Shuai Wang, and Ping Yang are with the Key Laboratory on Adaptive Optics, Chinese Academy of Sciences, Chengdu 610209, China, and also with the Institute of Optics and Electronics, Chinese Academy of Sciences, Chengdu 610209, China (e-mail: zlcheng911@163.com; zw2017@foxmail.com; gaozeyu1994@hotmail.com; yangkangjian@ioe.ac.cn; wangshuai@ioe.ac.cn; pingyang2516@163.com).

Digital Object Identifier 10.1109/JPHOT.2022.3203993

the wavefront has higher compatibility and applicability in most of AO systems. From the perspective of network model, for dealing with the time series prediction problem of wavefront prediction, LSTM network has more advantages under the same environment configuration [23]. This is because LSTM network has a strong memory ability and can accurately learn the temporal features between successive distorted wavefront frames to meet the prediction requirements. However, due to the temporal features of continuous wavefront, the direct feature extraction from the unrefined continuous wavefront will cause redundant errors, which damages the prediction accuracy. Therefore, a deep learning-based RLFNet is proposed for the first time in this paper, which eliminates the redundant information between frames by means of residual learning, then extracts the refined features for fusion, and fuses the features at all levels again to obtain a high accuracy prediction result. The prediction performance of our proposed RLFNet is tested from simulation and experiment results under different types of atmospheric turbulence conditions.

II. Atmospheric Simulation and Network Setup

A. Atmospheric Turbulence Distorted Wavefront Simulation

The atmospheric frozen flow hypothesis is a widely adopted modeling approach for atmospheric turbulence that has been verified by a large number of experiments [24], [25], [26], [27]. It has been shown that the time scale on which the frozen flow hypothesis holds is 10∼20 ms, reaching 50∼100 ms in a few cases [28]. In the AO system with a sampling frequency of more than 1 kHz, the time delay of the system is basically less than 3 ms, so the frozen flow hypothesis in such a system is reasonable.

Atmospheric turbulence occurs on a cascade of spatial scales with a power law dependence well approximated by Kolmogorov's Law [29], that is, the refractive index structure function in the inertial region satisfies the "two-thirds law", which is expressed as:

$$D_n\ (r) = C_n^2\ (h)\, r^{2/3} \tag{1}$$

Where: r is the scalar distance, C_n^2 is the refractive index structure constant changing with altitude h. As a statistical model, the expression of the classical model HV-57 is as follows:

$$C_n^2\ (h) = 5.94 \times 10^{-53} \left(\frac{v}{27}\right)^2 h^{10} \exp\left(-\frac{h}{1000}\right) + 2.7 \times 10^{-16} \exp\left(-\frac{h}{1500}\right) + A \exp\left(-\frac{h}{100}\right) \tag{2}$$

Among them, generally take: $v = 21m/s$, $A = 1.7 \times 10^{-14}$. The formula shows that atmospheric turbulence is the strongest at near the ground. As the altitude increases, C_n^2 experiences a process that will first become weaker, then stronger, and finally gradually weaken.

In laser atmospheric transmission and AO correction technology, D/r_0 is widely used to describe the influence of turbulence effects. where D is the diameter of the telescope, and the r_0 is the Fried parameter. The larger the value of r_0, the better the atmospheric conditions. In general, the relationship between r_0 and C_n^2 is [30]:

$$r_0 = \left[0.423k^2 sec\varphi \int_0^L C_n^2\,(z)\, dz\right]^{-3/5} \tag{3}$$

Where k is the wavenumber, L is the transmission distance, and φ is the zenith angle.

If the horizontal transmission, i.e., $\varphi = 0$, the above equation can be simplified as:

$$r_0 = 1.68\left(C_n^2 L k^2\right)^{-3/5} \tag{4}$$

The variation of wind speed with altitude in the atmosphere is often expressed by the Buffton wind speed model, as:

$$v\ (h) = v_g\ + v_t \times \exp\left(-\left(\frac{h - h_{pk}}{h_{scale}}\right)^2\right) \tag{5}$$

Among them, generally take: $v_g = 5\,m/s$, $v_t = 30\,m/s$, $h_{pk} = 9400$, $h_{scale} = 4800$.

In this paper, the simulation data is generated by the time evolution of the Fourier series method based on the above atmospheric turbulence theory. We simulate the distorted wavefront according to the experimental scene of the 1 km near-ground laser atmospheric near-horizontal transmission system. Since the recovery accuracy of SHWS is limited, the phase screen has more detailed phase structure information than the wavefront recovered by SHWS, therefore, we use the phase screen as the training data of our proposed RLFNet, which can improve the generalization of the network model.

B. Network Model Setup

The principle of our proposed RLFNet applied to the AO system is shown in Fig. 1. The SHWS is used to detect the slope information of the wavefront, and then after wavefront reconstruction, the control signal is output by the control system with prediction model to drive the DM to produce deformation, so as to compensate the actual distorted wavefront. In this paper, we focus only on the implementation of the wavefront prediction neural network model, which belongs to the open-loop prediction process, so the present study procedure is shown by the solid black arrows.

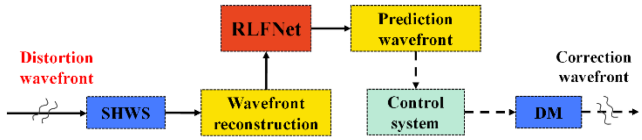

Fig. 1. AO system with wavefront prediction model.

There are five key points in building a supervised network model: input, output, loss function, label, and model structure [31]. There is a trade-off between the network prediction time and the number of wavefront predicted by the output. In order to accommodate to the time delay of 2∼3 sampling periods in most AO systems, in our RLFNet, we use consecutive wavefront

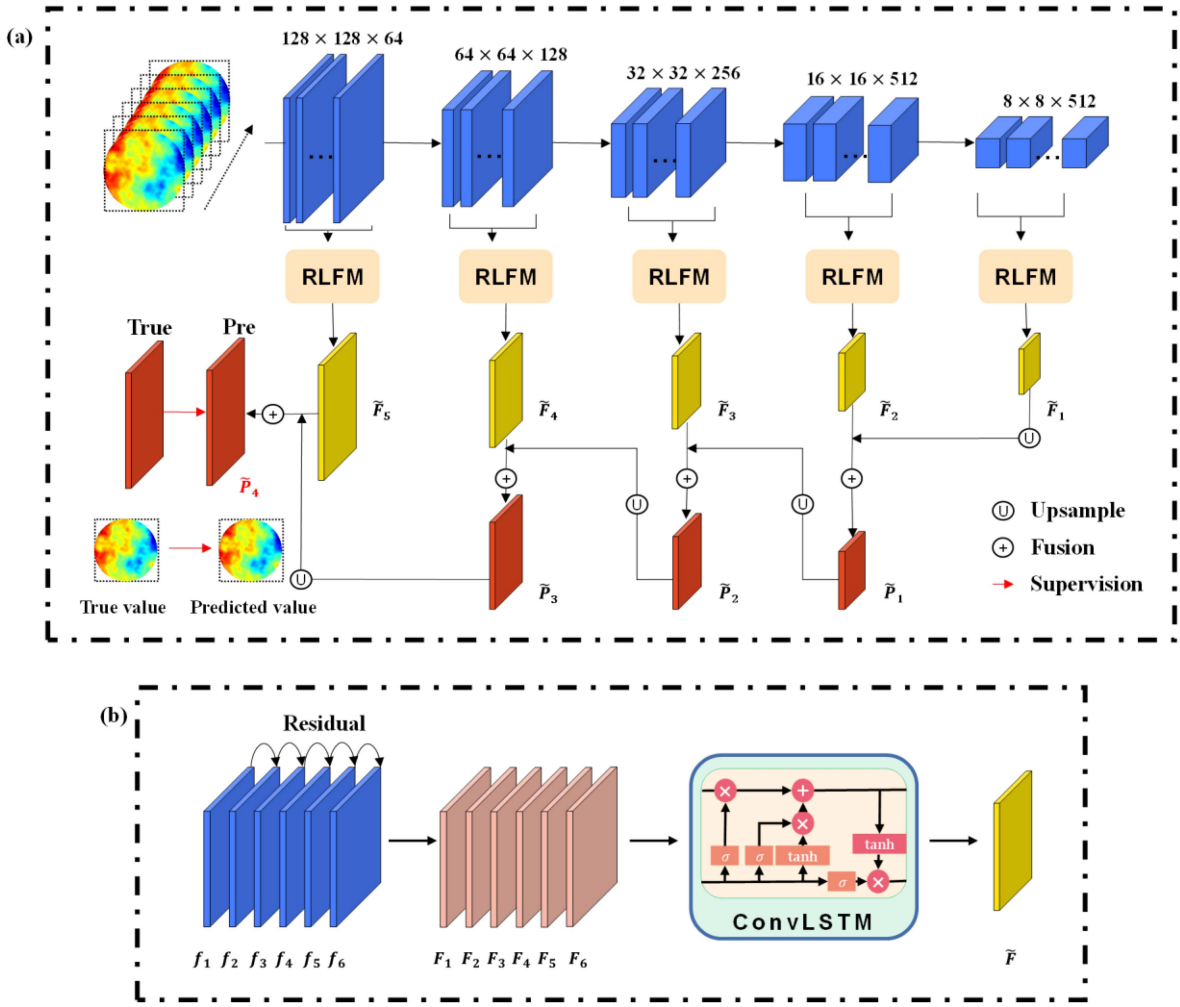

Fig. 2. The model architecture of our proposed RLFNet. (a). The schematic diagram of the structure of our proposed RLFNet. (b). The schematic diagram of our proposed RLFM.

of the first n frames as few as possible to predict the wavefront of the n+2 frame. In order to select the most suitable network input, we take n as 3, 4, 5, 6 and 7 respectively. We found that when the input is 6 consecutive frames and later, the accuracy of wavefront prediction remains basically unchanged. Considering that more wavefront inputs tend to bring the problem of excessive computation and the risk of overfitting, we finally selected 6 consecutive frames as the final input of our proposed network. That is, the continuous wavefront from time t to t+5 is used as the input of the network, and the distorted wavefront at moment t+7 is used as the output. Such an input-output setting can effectively avoid both the problem of too much data being processed by the network in a single pass and the wavefront latency for subsequent DM compensation. The loss function of our network model uses the $L1\_loss$ function, as follows:

$$L1\_loss = \sum_{i} \left| y(i)_{predict} - y(i)_{true} \right| \tag{6}$$

Where $y(i)_{predict}$ is the predicted value of the distorted wavefront at moment t and $y(i)_{true}$ is true value of the distorted wavefront at moment t. The $L1\_loss$ function is used in our model to minimize the sum of all the absolute value errors between the true value and the predicted value. The smaller the value of $L1\_loss$, the closer the predicted value is to the true value, which means that the prediction effect is better and the residual RMS (RMSe) value between the predicted value and the true value is smaller. Therefore, we choose RMSe as the evaluation index of the prediction performance of our proposed RLFNet.

In our proposed RLFNet, as shown in Fig. 2(a), VGG19 [32] is used as the backbone network, there is a residual learning fusion module (RLFM) in our RLFNet. The redundant information between two adjacent frames is eliminated by means of residual learning, and then the refined features are extracted for fusion. The process is shown as follows:

$$F_I = \sigma\left(\omega_1 * Concat\left(f_i, f_{i+1}\right) + b_1\right) + f_i \tag{7}$$

Where σ represents the activate function, i.e., PReLU [33], $Concat(\ldots,\ldots)$ represents the concatenation operation [34], (ω_1, b_1) denotes the weight and bias of a 1×1 convolutional layer, and "$*$" means convolutional operation.

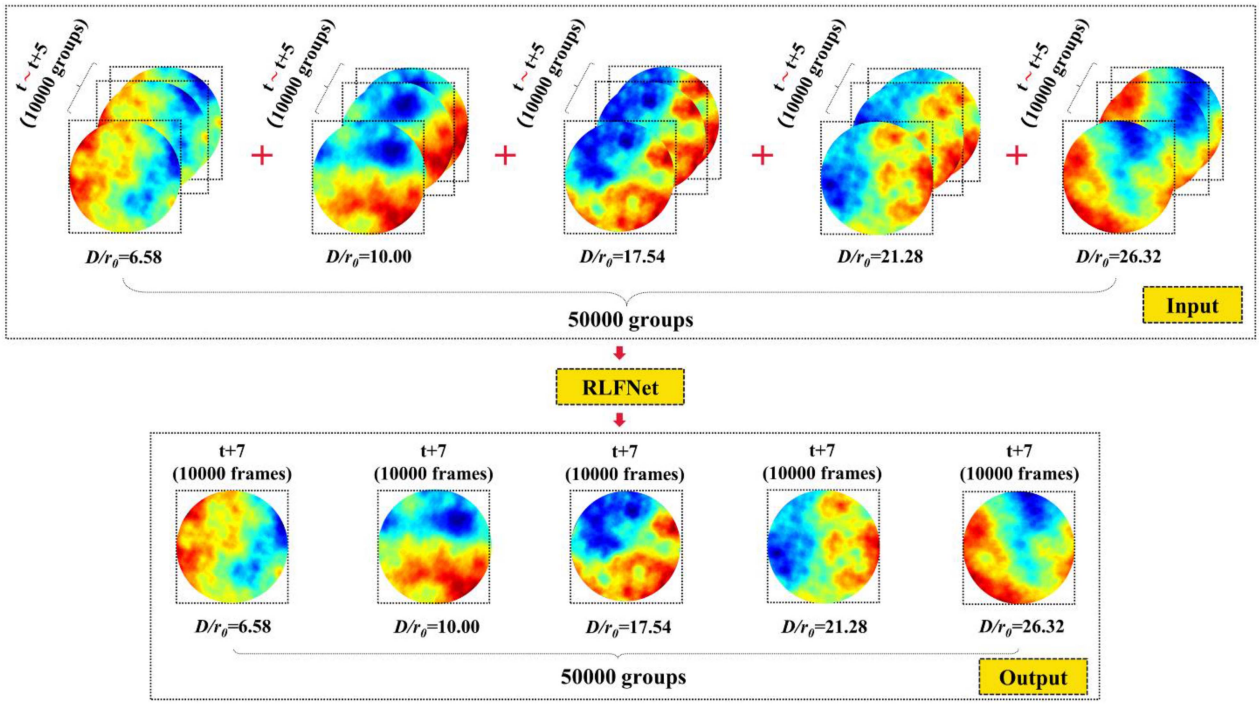

Fig. 3. The input and output settings of the training dataset of our proposed RLFNet.

We use the memory capability of the Convolutional Long Short-term Memory (ConvLSTM) network [35] to predict the output wavefront information at moment t+7 based on the continuous wavefront features from t to t+5, as shown in Fig. 2(b). Finally, the features at all levels are fused again to obtain the final prediction results. The process is shown as follows:

$$\tilde{P}_1 = \sigma\left(\omega_2 * Concat\left(\tilde{F}_1, \tilde{F}_2\right) + b_2\right) \quad (8)$$

$$\tilde{P}_2 = \sigma\left(\omega_3 * Concat\left(\tilde{F}_2, \tilde{F}_3\right) + b_3\right) \quad (9)$$

$$\tilde{P}_3 = \sigma\left(\omega_4 * Concat\left(\tilde{F}_3, \tilde{F}_4\right) + b_4\right) \quad (10)$$

$$\tilde{P}_4 = \sigma\left(\omega_5 * Concat\left(\tilde{F}_4, \tilde{F}_5\right) + b_5\right) \quad (11)$$

Where (ω_2, b_2), (ω_3, b_3), (ω_4, b_4), and (ω_5, b_5) denote the weights and bias of a 1×1 convolutional layer. The final predicted value is $\tilde{P}_4$.

III. Numerical Simulation and Discussion

A. Data Generating

We use different values of D/r_0 to simulate the distorted wavefront with different atmospheric turbulence conditions, D is set to 1m and the sampling frequency is set to 1 kHz. According to the experimental environment, in the simulation, we set the wavelength to 1064nm and considered five turbulent layers, each of which is evenly distributed within 1km of the transmission path and located in the middle of each segment. At the transmit/receive altitude of about 10 m near the ground, the wind speed is set to about 5.65 m/s, and the wind direction is set randomly 0∼120 degrees to increase the diversity. According to (2), at this time, C_n^2 is a certain value, that is $C_n^2 = 1565e-17$. However, in practice, it will be mainly affected by temperature gradients under different weather conditions [36]. The experimental measurement analysis shows that the variation of C_n^2 in the area where our experimental system is located is generally about an order of magnitude [36]. Therefore, according to (4), five increased C_n^2 values are selected in this range, that is, $0.1C_n^2$, $0.2C_n^2$, $0.5C_n^2$, $0.7C_n^2$ and $1.0C_n^2$ to simulate the atmospheric turbulence intensity under different r_0 conditions. The values of r_0 are 0.152, 0.100, 0.057, 0.047, and 0.038, that is, D/r_0 are 6.58, 10.00, 17.54, 21.28, and 26.32, respectively.

We input the simulated 5 groups of distorted wavefronts under different D/r_0 into our proposed RLFNet at the same time to improve the robustness of the network. For each dataset, we used the continuous wavefront from time t to t+5 as the input to the network, and the distorted wavefront at moment t+7 as the label. 10500 groups of data were generated under each D/r_0 condition, among which the first 10000 groups were used as training frames and the last 500 groups were reserved to test the performance of the model. That is, a total of 50000 groups of data were used as our training dataset. This splitting of the training and test dataset prevents the network model from learning the input information of unknown data in advance. Fig. 3 more clearly represents the input and output settings of the training dataset of our proposed RLFNet.

B. Analysis of Simulation Results

The prediction performance of our proposed RLFNet at different D/r_0 has been tested after training the network model. We obtained the wavefront at the corresponding moment t+7 from the continuous wavefront data at time t to t+5 in the simulated

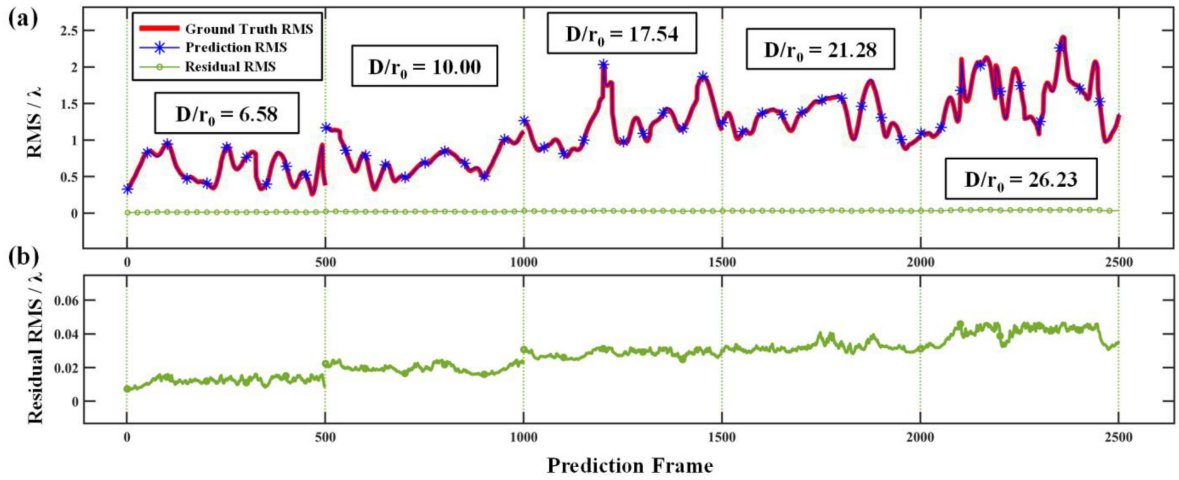

Fig. 4. The simulation results of our proposed RLFNet. (a) The RMS values of the predicted and true values of all frames within the test dataset. (b) The residual RMS of the predicted and true values of all frames within the test dataset.

TABLE I
SIMULATION DATA RESULTS DISPLAY

r_0 (m)	D/r_0	Truth RMS (λ)	Prediction RMS (λ)	RMSe (λ)	RMSe/Truth RMS	SSIM
0.152	6.58	0.6039	0.6025	0.0122	**2.0%**	0.9603
0.100	10.00	0.7303	0.7323	0.0196	**2.7%**	0.9455
0.057	17.54	1.2141	1.2181	0.0284	**2.3%**	0.9530
0.047	21.28	1.3056	1.3114	0.0321	**2.5%**	0.9508
0.038	26.32	1.5853	1.5857	0.0403	**2.5%**	0.9305

test dataset and compared it with the pre-prepared labeled dataset for analysis.

The RMSe of all frames within the test dataset to characterize the prediction performance of our proposed RLFNet, as shown in Fig. 4. In addition to that, we also employed the structural similarity function (SSIM) to verify the structural similarity of the prediction results with the real wavefront. Table I shows the RMS value of the original distorted wavefront (Truth RMS), the RMS value of the predicted distorted wavefront (Prediction RMS), the RMSe, the ratio of the RMSe to Truth RMS (RMSe/Truth RMS), and the SSIM for each test dataset. This result is based on the average of all 500 frames from each test dataset.

The above results show that the larger the D/r_0, the stronger the atmospheric turbulence intensity, and the larger the RMSe. But the RMSe/Truth RMS is basically stable at around 2.5%. This indicates that our proposed RLFNet has a well prediction performance of the distorted wavefront at different turbulence intensities.

C. Ablation Studies

We conducted several ablation studies to demonstrate the effectiveness of each component of our proposed RLFNet. The two methods are built by removing the main part of our RLFNet, respectively. The two methods used exactly the same training dataset and test dataset as our RLFNet, the average RMSe value and SSIM under different methods are intuitively shown in Fig. 5.

More specifically, by comparing the results of the first method without residual learning (expressed as *w/o* residual-learning) with our RLFNet, we can clearly observe that the results of the *w/o* residual-learning method are less accurate than those of our RLFNet. This fully demonstrates that residual learning can effectively improve the prediction performance. Secondly, in order to verify the validity of ConvLSTM, the ConvLSTM part was removed from RLFNet and the predicted wavefront was obtained by general convolution method to ensure the consistency of input/output dimensions. The method of removing ConvLSTM (represented as *w/o* ConvLSTM) was compared with our proposed method, and results showed that *w/o* ConvLSTM performed worse. This shows that ConvLSTM can use its strong memory ability to well fuse the historical distorted wavefront information with temporal features and obtain better prediction results. The RMSe/RMS_Ture results of these methods are compared in Table II, which further demonstrates that each component of our proposed method contributes to the final prediction results.

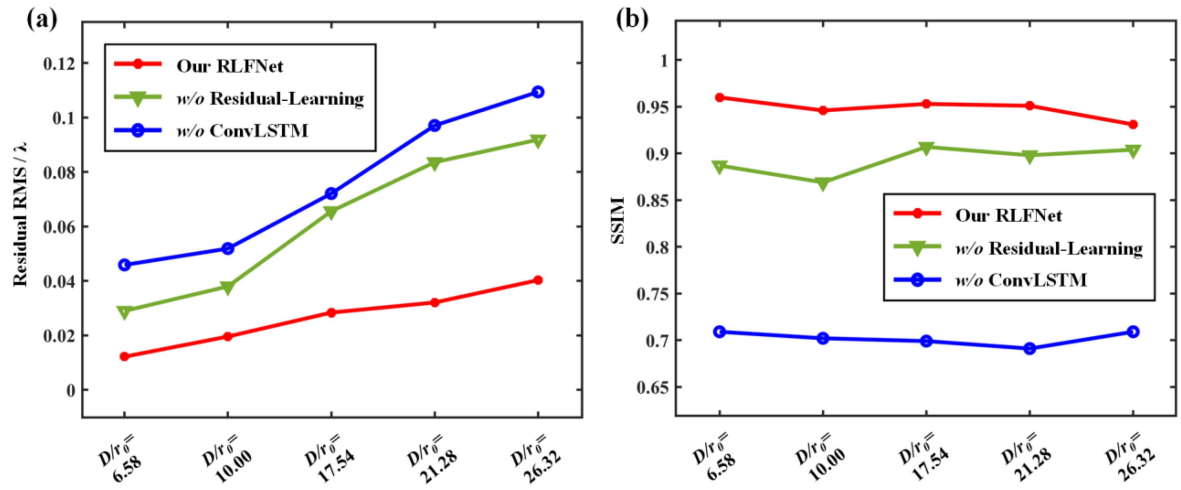

Fig. 5. The results of the ablation studies. (a) The average RMSe value under different methods. (b) The SSIM under different methods.

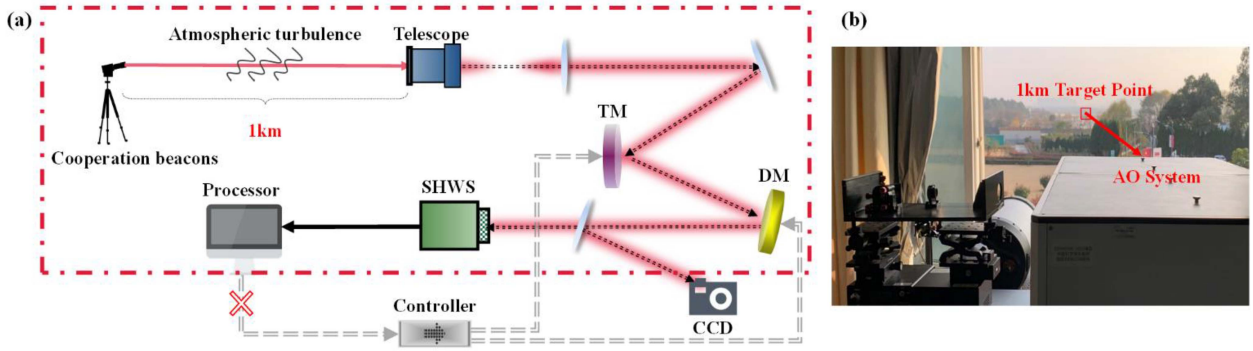

Fig. 6. The 1km laser atmospheric transmission system. (a) The schematic diagram of the experimental operating system. (b) Experimental system actual installation.

TABLE II
COMPARISON OF THE RMSE/RMS_TURE RESULTS BY DIFFERENT MODULES IN ABLATION STUDIES

Methods		Our RLFNet	*w/o* residual-learning	*w/o* ConvLSTM
D/r_0=6.58	RMSe/Truth RMS	**2.0%**	4.8%	7.6%
D/r_0=10.00	RMSe/Truth RMS	**2.7%**	5.2%	7.1%
D/r_0=17.54	RMSe/Truth RMS	**2.3%**	5.4%	8.0%
D/r_0=21.28	RMSe/Truth RMS	**2.5%**	6.4%	8.3%
D/r_0=26.32	RMSe/Truth RMS	**2.5%**	5.8%	6.9%

IV. EXPERIMENTAL VERIFICATION

A. Analysis of Experimental Results

Our proposed RLFNet performance was tested on data collected by the 1km laser atmospheric transmission system, where the laser source is a cooperative target and the collection method is one-shot open-loop. The schematic diagram of the experimental operating system for laser atmospheric transmission and the experimental setup is shown in Fig. 6. The laser emitted from the cooperative beacons first enters the telescope, which is reoriented by the tilt mirror (TM) and subsequently corrected for aberration by the DM. The beam is divided into two beams by the spectroscope, one of which is directly output to the Charge Coupled Device (CCD), and the other into the SHWS, which measures the aberration. In this paper, we are committed to the prediction of the distorted wavefront, and do not conduct closed-loop correction experiments, so the experimental data are derived from a one-shot open-loop collection of the system, as shown in the red dashed box in Fig. 6.

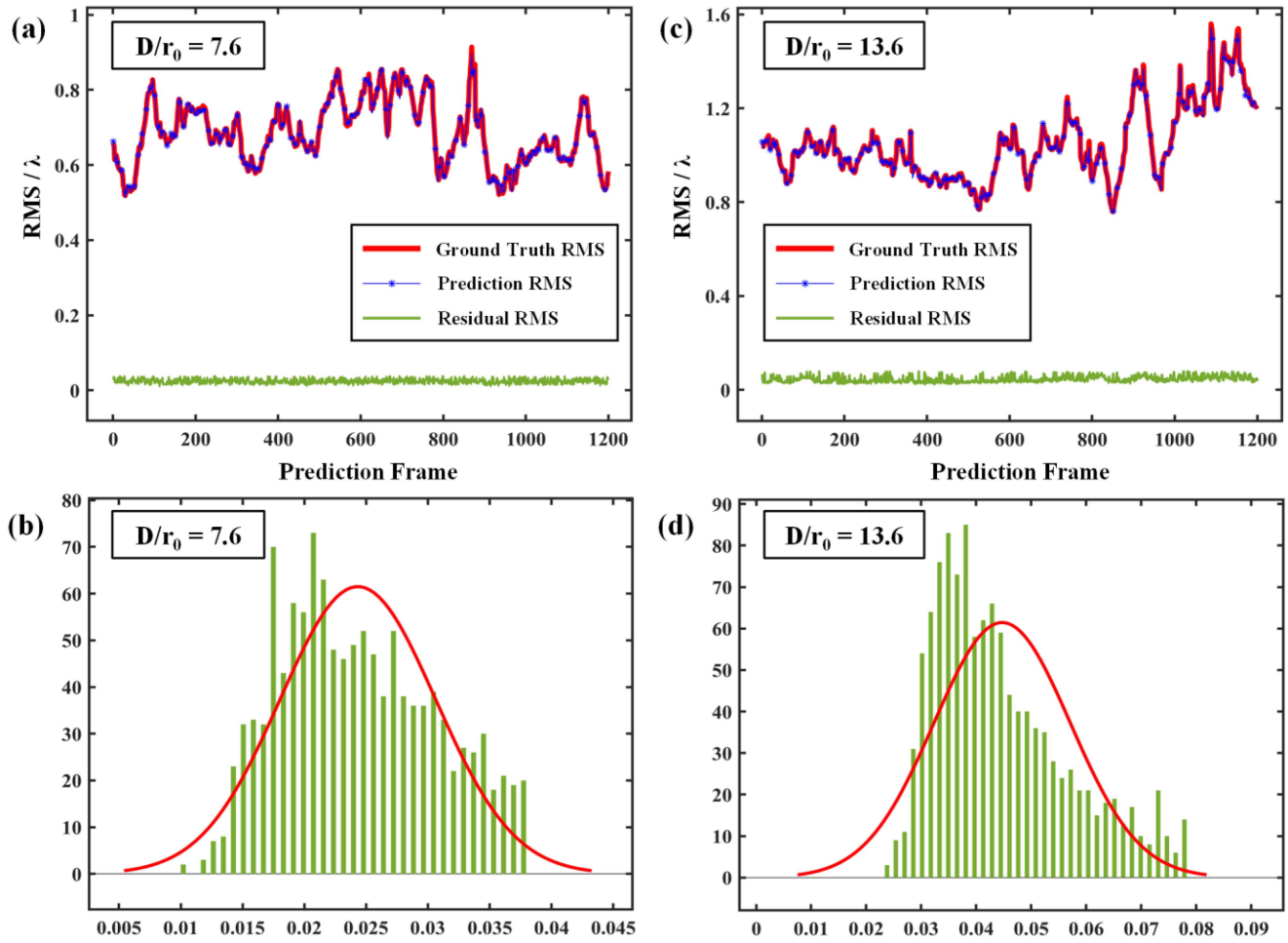

Fig. 7. The experimental results of our proposed RLFNet. (a-b) When the D/r_0 is 7.6, the comparison of RMS of all frames in the experimental test dataset and the probability distribution of the residual RMS. (c-d) When the D/r_0 is 13.6, the comparison of RMS of all frames in the experimental test dataset and the probability distribution of the residual RMS.

We were provided with two groups of SHWS data with D/r_0 of 7.6 and 13.6, both with a frame rate of 1 kHz and both with a collection time of 10s. The relevant parameters of the cooperative target and wavefront sensor in the experiment, as well as the data estimated for some atmospheric conditions, are shown in Table III. We used the mode method [37] for wavefront recovery of SHWS data. In the recovery process, it was found that when the zernike mode exceeded 104, the sum of the absolute values of the zernike coefficients of each frame remains roughly the same. Therefore, we only applied 104-order Zernike mode for wavefront recovery of experimental data according to experimental parameters. Since the beam jitter has been suppressed by the TM based on CCD information during open-loop data acquisition, the aberration of tilt and tip are not considered in the wavefront recovery.

TABLE III
THIS IS A SAMPLE OF A TABLE TITLE

Parameter	Value
Subapertures	14*14
Pixel resolution	128*128
Aperture diameter	0.28 m
Wavelength	1064 nm
Wind Speed	3.4-5.4 m/s
Frame rate	1 kHz
Transmit/receive altitude	10 m
Transmission distance	1 km

The presentation of the results for the two groups of experimental data is based on a fine-tuned model. Fine-tuning is a process in which a limited portion of a pre-trained network is retrained on a particular dataset to improve its specificity to this dataset [38]. This is because the nature of simulated data is quite dissimilar from our experimental data, in that they are noiseless models of frozen, discrete layers. The training of fine-tuning is very fast due to the fact that the pre-trained network model has learned the laws of feature extraction and successfully identified the frozen flow part of the experimental data. We set aside

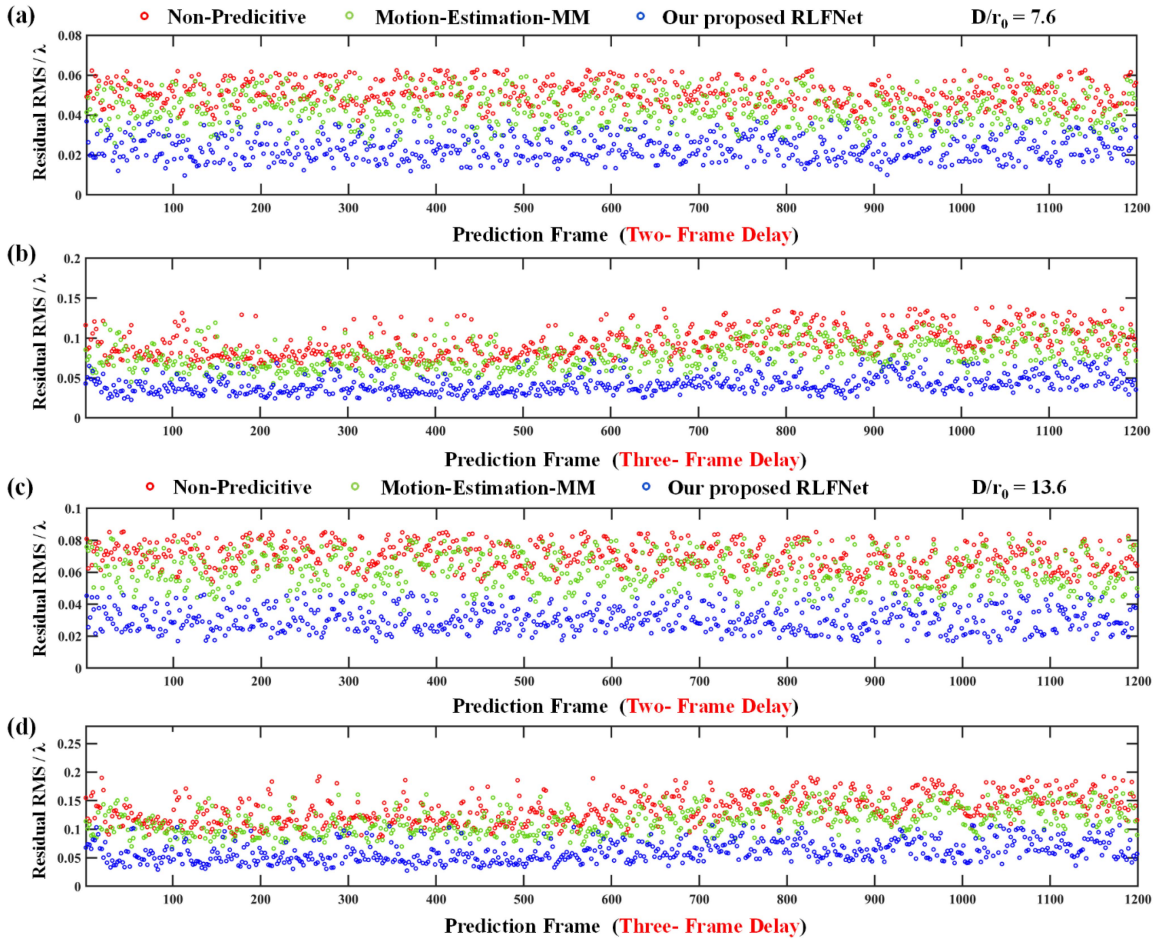

Fig. 8. The results of the comparative experiment. (a-b) When the D/r_0 is 7.6, in the case of two-frame latency and three-frame latency, the RMSe of two comparison experiments and our proposed RLFNet. (c-d) When the D/r_0 is 13.6, in the case of two-frame latency and three-frame latency, the RMSe of two comparison experiments and our proposed RLFNet.

TABLE IV
EXPERIMENTAL DATA RESULTS DISPLAY

D/r_0	Truth RMS (λ)	Prediction RMS (λ)	RMSe (λ)	RMSe/Truth RMS	SSIM
7.6	0.6872	0.6876	0.0237	**3.4%**	0.974
13.6	1.1175	1.1163	0.0426	**3.8%**	0.955

1200 frames of data as a test dataset and did not participate in the training process, so the test dataset was not trained in advance. Fig. 7 shows the comparison of RMS of all frames in the two experimental test dataset and the probability distribution of RMSe.

Table IV shows the Truth RMS, the RMSe, the RMSe/Truth RMS and the average SSIM for the two groups of experimental data. Again, this result is based on the average of all 1200 frames within the test dataset.

B. Comparative Experiment

In order to verify the prediction performance of our proposed RLFNet method, we conducted two groups of comparative experiments. One group is a non-predictive method and the other is a linear predictive method. The non-predictive method is also done in a one-shot open-loop condition, where only the recently collected wavefront is used to compensate for future frames, regardless of delay. In other words, two-frame latency system in which the wavefront collected at the moment *t-2* is used to compensate the frame at the most recent moment *t*. We also conducted tests under the assumption of three-frame latency system. Similarly, the three-frame latency system uses the wavefront collected at the history moment *t-3* directly to compensate for the wavefront at the most recent moment *t*. The linear predictive method to be compared in this paper is based on the motion-estimation algorithm of module matching (Motion-Estimation-MM). The motion direction of atmospheric

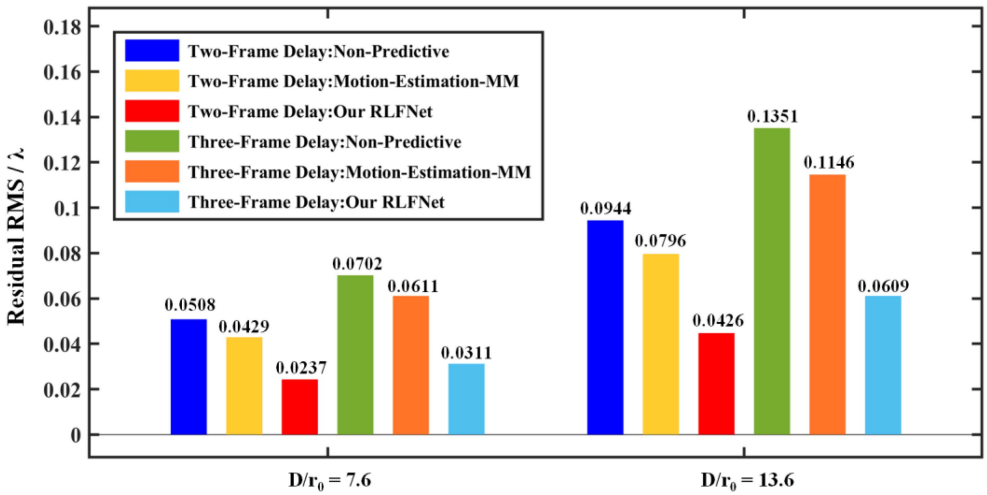

Fig. 9. Performance comparison of two methods with our proposed RLFNet.

turbulence is estimated according to the wavefront recovery image of the reference frame and the current frame, and then the current frame is mobile-processed to predict the image of the future frame [16]. This Motion-Estimation-MM adopts the search strategy and matching criteria of Adaptive Cross Pattern Search (ARPS) algorithm [39].

We use the same test dataset and prediction strategy to test the two methods and compare them with our proposed RLFNet. Fig. 8 shows the RMSe of all the same frames in the test dataset of the two groups of comparison experiments and our proposed RLFNet.

As can be seen from the test results of the comparative experiments:

a) Our proposed RLFNet has a well prediction performance of the distorted wavefront for different atmospheric turbulence conditions. It proves that our network has a good generalization capability, however, there is a slight degradation in performance compared with the simulation data, which is due to the uncertainty and randomness error of the experimental data, as mentioned above.
b) The prediction performance of our proposed RLFNet and Motion-Estimation-MM is better than the non-predictive method, and our proposed RLFNet performs best because the matching degree between the wavefront aberrations detected by Motion-Estimation-MM and the frozen flow hypothesis is uncertain, so it is difficult to adapt to the changeable turbulence conditions.

As shown in the Fig. 9, we compared the average RMSe of all frames in the test dataset for the three methods. In the two-frame latency system, when the D/r_0 is 7.6, the average RMSe of our proposed RLFNet is 0.0237λ, and the average RMSe of Motion-Estimation-MM is 0.0429λ. Compared with the non-predictive method, the average RMSe of Motion-Estimation-MM decreases about 15.6%, however, our proposed RLFNet decreases about 53.3%. When the D/r_0 is 13.6, the average RMSe of Motion-Estimation-MM decreases about 15.7%, however, our proposed RLFNet decreases about 54.9%. When our network is applied to a three-frame latency system, although the average RMSe decreases, it shows a better performance improvement. When the D/r_0 is 7.6, the average RMSe of our proposed RLFNet decreases about 55.7%, but the Motion-Estimation-MM decreases only about 13.0%. When the D/r_0 is 13.6, the average RMSe of our proposed RLFNet decreases about 54.9%, but the Motion-Estimation-MM decreases only about 15.2%.

It can be seen that our proposed RLFNet performs better when the atmospheric turbulence is stronger, which is due to the fact that when the atmospheric turbulence intensity is stronger, the difference in structural similarity between two adjacent frames is larger, and this is why our proposed RLFNet shows a better performance. When the time delay of the system increases, the difference between the compensated wavefront and the actual wavefront also becomes larger, so our network performs better in the three-frame latency system instead. Therefore, we believe that there will be better performance improvements if the network can predict up to frame t+8, which will be implemented in the following work.

V. Conclusion

In this paper, we propose a novel wavefront prediction method based on residual learning fusion network with high accuracy, which aims to solve the latency problem of the traditional AO system. The method eliminates the redundant information between adjacent distorted wavefront frames due to temporal features by residual learning, and then fuses the refined features at all levels to obtain the predicted wavefront. The simulation results show its effectiveness and generalization ability, and its performance is testified from data collected on the 1km laser transmission atmospheric transmission experimental setup. The results show that the proposed method leads to an average RMSe reduction up to 53% for both different atmospheric turbulence conditions compared to the non-predicted method. Proposed method has potential to solve latency problem in a close-loop AO system, which can improve correction bandwidth significantly.

REFERENCES

[1] G. Sivo, C. Kulcsár, and J.-M. Conan, "First on-sky SCAO validation of full LQG control with vibration mitigation on the CANARY pathfinder," *Opt. Exp.*, vol. 22, no. 19, pp. 23565–23591, 2014.

[2] D. L. Fried, "Time-delay-induced mean-square error in adaptive optics," *JOSA A*, vol. 7, no. 7, pp. 1224–1225, Jul. 1990.

[3] C. Kulcsár, H.-F. Raynaud, and C. Petit, "Minimum variance prediction and control for adaptive optics," *automatica*, vol. 48, no. 9, pp. 1939–1954, Sep. 2012.

[4] Z. J. Yan, X. Y. Li, and C. H. Rao, "Numerical simulation of a prediction control algorithm for close-loop adaptive optical system," *Acta Optica Sinica,* vol. 31, no. 1, Jan. 2011, Art. no. 0101003.

[5] C. Liu, L. F. Hu, and Q. Q. Mu, "Modal prediction for open-loop liquid-crysta adaptive optics systems," *Acta Physica Sinica*, vol. 61, no. 12, 2012, Art. no. 129501, doi: 10.7498/aps.61.129501.

[6] M. D. Wiberg, C. E. Max, and D. T. Gavel, "A spatial non-dynamic LQG controller: Part I, application to adaptive optics," in *Proc. 43rd IEEE Conf. Decis. Control*, 2004, pp. 3326–3332.

[7] M. D. Wiberg, C. E. Max, and D. T. Gavel, "A spatial non-dynamic LQG controller: Part II, theory," in *Proc. 43rd IEEE Conf. Decis. Control*, 2004, pp. 3333–3338.

[8] P. Douglas, "Linear-quadratic-Gaussian control for adaptive optics systems using a hybrid model," *JOSA A*, vol. 26, no. 1, pp. 1–9, Dec. 2009.

[9] C. Petit et al., "Kalman-filter-based control for adaptive optics," in *Proc. Advancements Adaptive Opt.*, Oct. 2004, pp. 1414–1425.

[10] M. Gray et al., "Local ensemble transform Kalman filter, a fast non-stationary control law for adaptive optics on ELTs: Theoretical aspects and first simulation results," *Opt. Exp..,* vol. 22, no. 17, pp. 20894–20913, Aug. 2014.

[11] P. Massioni, C. Kulcsár, H.-F. Raynaud, and J.-M. Conan, "Fast computation of an optimal controller for large-scale adaptive optics," *J. Opt. Soc. Amer. A*, vol. 28, no. 11, pp. 2298–2309, Oct. 2011.

[12] L. Poyneer, B. A. Macintosh, and J. Véran, "Fourier transform wavefront control with adaptive prediction of the atmosphere," *JOSA A*, vol. 24, no. 9, pp. 2645–2660, Jul. 2007.

[13] L. C. Johnson, D. T. Gavel, and D. M. Wiberg, "Bulk wind estimation and prediction for adaptive optics control systems," *JOSA A,* vol. 28, no. 8, pp. 1566–1577, Jul. 2011.

[14] O. Guyon and J. Males, "Adaptive optics predictive control with empirical orthogonal functions (EOFs)," Jul. 2017, *arXiv: 1707.00570*.

[15] L. Poyneer and J.-P. Véran, "Predictive wavefront control for adaptive optics with arbitrary control loop delays," *JOSA A*, vol. 28, no. 8, pp. 1486–1496, Jun. 2008.

[16] X. Zhou and X. Y. Li, "Wavefront distortion prediction method based on motion estimation," *Opto-Electron. Eng.*, vol. 48, no. 10, 2021, Art. no. 210288.

[17] M. A. Chen, X. Q. Jin, S. B. Li, and Z. Y. Xu, "Compensation of turbulence-induced wavefront aberration with convolutional neural networks for FSO systems," *Chin. Opt. Lett.*, vol. 19, no. 11, Nov. 2021, Art. no. 110601.

[18] Y. M. Guo et al., "Adaptive optics based on machine learning: A review," *Opto-Electron. Adv.*, vol. 5, 2022, Art. no. 200082.

[19] J. G. Chen, V. Shah, and L. L. Liu, "Performance of a U-Net-based neural network for predictive adaptive optics," *Opt. Lett.*, vol. 46, no. 10, pp. 2513–2516, May 2021.

[20] X. Y. Shi, Y. Feng, and Y. Chen, "Predicting control voltages of deformable mirror in adaptive optics system," *High Power Laser Part. Beams,* vol. 24, no. 6, pp. 1281–1286, Jun. 2012.

[21] Z. J. Yan and X. Y. Li, "Neural network prediction algorithm for control voltage of deformable mirror in adaptive optical system," *Acta Optica Sinica*, vol. 30, no. 4, pp. 911–916, Apr. 2010.

[22] Y. Chen, "Voltages prediction algorithm based on LSTM recurrent neural network," *Optik*, vol. 220, no. 16, pp. 4869–4880, Oct. 2020.

[23] P. Lara-Benítez, M. Carranza-García, and J. C. Riquelme, "An experimental review on deep learning architectures for time series forecasting," *Int. J. Neural Syst.*, vol. 31, no. 3, Feb. 2021, Art. no. 2130001.

[24] S. Matthias and J. Earl, "Method for a quantitative investigation of the frozen flow hypothesis," *JOSA A*, vol. 17, no. 9, pp. 1650–1658, Sep. 2000.

[25] L. Poyneer, M. V. Dam, and J. P. Véran, "Experimental verification of the frozen flow atmospheric turbulence assumption with use of astronomical adaptive optics telemetry," *JOSA A*, vol. 26, no. 4, pp. 833–846, Mar. 2009.

[26] E. Gendron and P. Léna, "Single layer atmospheric turbulence demonstrated by adaptive optics observations," *Astrophys. Space Sci.*, vol. 239, no. 2, pp. 221–228, Sep. 1996.

[27] B. Kern, T. A. Laurence, C. Martin, and P. E. Dimotakis, "Temporal coherence of individual turbulent patterns in atmospheric seeing," *Appl. Opt.*, vol. 39, no. 27, pp. 4879–4885, Sep. 2000.

[28] Z. H. Li and X. Y. Li, "Performance of predictive correction foe adaptive optics systems with frozen flow turbulence," *Opt. Precis. Eng.*, vol. 26, no. 3, pp. 548–555, 2018.

[29] A. N. Kolmogorov, "The local structure of turbulence in incompressible viscous fluid for very large reynolds numbers[J]," *Proc. Roy. Soc. London. Ser. A: Math. Phys. Sci.*, vol. 434, no. 1890, pp. 9–13, 1991.

[30] J. Y. Wang, X. C. Liu, R. Z. Rao, and Z. B. Gong, "Measurement of atmospheric coherence length in daytime and at night," *High Power Laser Part. Beams*, vol. 16, no. 1, pp. 1–4, 2004.

[31] W. D. Xiang, P. Yang, S. Wang, B. Xu, and H. Liu, "Underwater image enhancement based on red channel weighted compensation and gamma correction model," *Opto-Electron. Adv.*, vol. 1, 2018, Art. no. 180024.

[32] K. He, X. Zhang, S. Ren, and J. Sun, "Delving deep into rectifiers: Surpassing human-level performance on imagenet classification," in *Proc. IEEE Int. Conf. Comput. Vis.*, 2015, pp. 1026–1034.

[33] K. Simonyan and A. Zisserman, "Very deep convolutional networks for large-scale image recognition," 2014, *arXiv:1409.1556*.

[34] S. Ma, N. Wang, L. C. Zhu, W. Shuai, Y. Ping, and X. Bing, "Light field depth estimation using weighted side window angular coherence[J]," *Opto-Electron. Eng.*, vol. 2021, vol. 48, no. 12, 2021, Art. no. 210405.

[35] X. Shi, Z. Chen, H. Wang, D. Yeung, W. Wong, and W. Woo, "Convolutional LSTM network: A machine learning approach for precipitation nowcasting," *Adv. Neural Inf. Process. Syst.*, vol. 28, pp. 802–810, 2015.

[36] G. Sun, N. Q. Weng, and L. M. Xiao, "Statistical characteristics of vertical distribution of atmospheric strucure constant of refractive index Cn2," *J. Atmos. Environ. Opt.*, vol. 6, no. 2, Mar. 2011.

[37] O. Soloviev and G. Vdovin, "Hartmann-Shack test with random masks for modal wavefront reconstruction," *Opt. Exp.*, vol. 13, no. 23, pp. 9570–9583, Nov. 2005.

[38] R. Girshick, J. Donahue, T. Darrell, and J. Malik, "Rich feature hierarchies for accurate object detection and semantic segmentation," in *Proc. IEEE Conf. Comput. Vis. Pattern Recognit.*, 2014, pp. 580–587.

[39] B. Biswas, R. Mukherjee, and I. Chakrabarti, "A high-speed VLSI architecture for motion estimation using modified adaptive rood pattern search algorithm," *Circuits Syst. Signal Process.*, vol. 37, no. 10, pp. 4548–4567, 2018.